

Electronic structure study by means of X-ray spectroscopy and theoretical calculations of the “ferric star” single molecule magnet

A. F. Takács* and M. Neumann

Universität Osnabrück – Fachbereich Physik, D-49069 Osnabrück, Germany

A. V. Postnikov†

Institut für Festkörperforschung, Forschungszentrum Jülich, D-52425 Jülich,

Germany and Russian Academy of Science – Ural Division,

S. Kovalevskoj 18, 620219 Yekaterinburg, Russia

K. Kuepper

Universität Osnabrück – Fachbereich Physik, D-49069 Osnabrück and Forschungszentrum Rossendorf,

Institut für Ionenstrahlphysik und Materialforschung,

Bautzner Landstrasse 128, 01328 Dresden, Germany

A. Scheurer, S. Sperner, and R. W. Saalfrank

Universität Erlangen–Nürnberg, Institut für Organische Chemie, D-91054 Erlangen, Germany

K. C. Prince

Sincrotrone Trieste, Strada Statale 14, km 163.5, in Area Science Park,

I-34012 Basovizza (Trieste), Italy and INFN-TASC,

Laboratorio ELETTRA, I-34012 Basovizza (Trieste), Italy

(Dated: November 21, 2005)

The electronic structure of the single molecule magnet system $\{M[Fe(L^1)_2]_3\} \cdot 4CHCl_3$ ($M = Fe, Cr$; $L^1 = CH_3N(CH_2CH_2O)_2^{2-}$) has been studied using X-ray photoelectron spectroscopy, X-ray absorption spectroscopy, soft X-ray emission spectroscopy, as well as theoretical density functional-based methods. There is good agreement between theoretical calculations and experimental data. The valence band mainly consists of three bands between 2 eV and 30 eV. Both theory and experiments show that the top of the valence band is dominated by the hybridization between Fe 3d and O 2p bands. From the shape of the Fe 2p spectra it is argued that Fe in the molecule is most likely in the 2+ charge state. Its neighboring atoms (O, N) exhibit a magnetic polarisation yielding effective spin $S=5/2$ per iron atom, giving a high spin state molecule with a total $S=5$ effective spin for the case of $M = Fe$.

PACS numbers: 75.50.Xx, 31.15.Ar, 33.20.Rm, 33.60.Fy

I. INTRODUCTION

In the quest for molecular magnets which might be useful for practical applications such as ultradense magnetic storage¹, quantum computing², or other interesting devices³, one finds at times molecules which combine structural beauty, promising chemistry for further development, non-trivial physics and practically interesting properties (intramolecular exchange interactions, magnetic anisotropy). Such new molecular materials often arise from metal-organic synthesis, which is the main driving force in studies of molecular magnets (see, e.g., the monograph by Kahn⁴, or Refs.^{5,6,7} for recent reviews). The present work is devoted to one such system, known as “ferric star”, which is simple enough to allow an accurate study of its electronic structure, yet far from trivial for what regards its chemical manipulation (crystallization with different ligands) and physical treatment (e.g., deposition on surfaces). The synthesis of magnetic molecules with the formula $\{M[Fe(L^1)_2]_3\} \cdot 4CHCl_3$, where $L^1 \equiv CH_3N(CH_2CH_2O)_2^{2-}$ is an organic ligand

and M is Fe or Cr, has been described by Saalfrank *et al.*⁸ (compounds **11** and **12** of this paper). Previous basic magnetochemical investigations of the “ferric star”⁹ indicate that the three spins $S=5/2$ of peripheral Fe ions at the star edges couple with an antiparallel orientation to the central ion, yielding (for $M = Fe$) the magnetic ground state of $S=5$. In the present work we attempt to clarify the electronic structure, as it emerges from a combined spectroscopic study and first-principles calculations.

Specifically, we probe core-level excitations of the ferric star at the L and other edges by several core spectroscopies, namely near-edge X-ray absorption spectroscopy (NEXAS), resonant inelastic X-ray scattering (RIXS) and X-ray photoemission spectroscopy (XPS). The electronic structure calculations were done from first principles within the density functional theory. The spectra give insight into the distribution of energy-resolved state densities within the valence band, which reveal the M 3d – O 2p hybridization, and into charge states of transition metal (TM) atoms. The calculations give estimates of local magnetic moments, spatial distribution of the spin

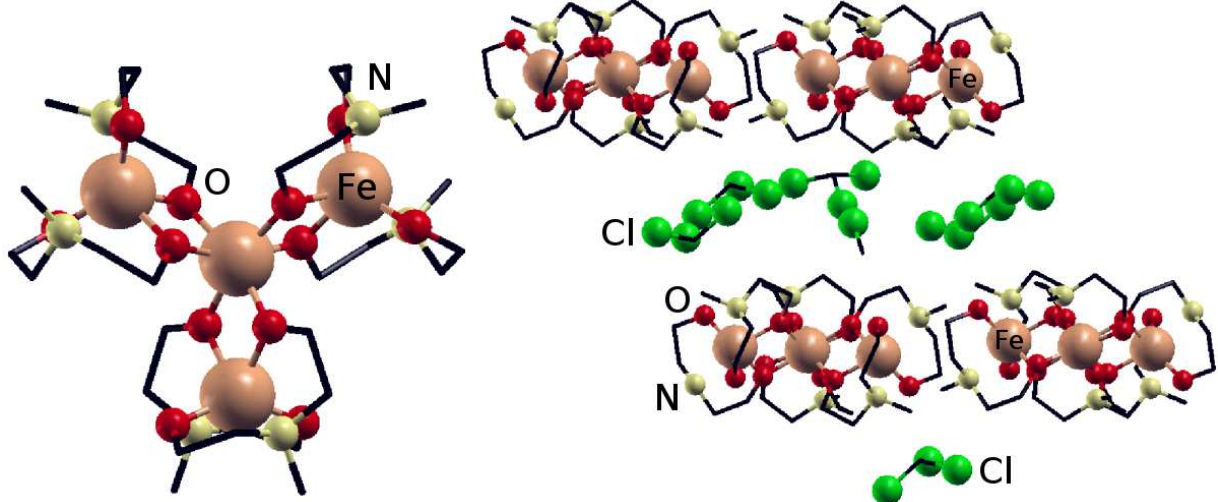


FIG. 1: Single “ferric star” molecule in the top view (left) and side view of the molecules packed in the crystal structure with chloroform (right). Hydrogen atoms are omitted, and carbon chains are shown as wireframe.

density, and of magnetic interaction parameters.

The paper is organized as follows. In Sec. II we summarize present knowledge of the crystal structure and basic magnetic properties. Sec. III gives technical details of the spectroscopy measurements, and of the first-principles electronic structure calculations. The discussion of results and comparison with the calculations is done in Sec. IV.

II. STRUCTURE AND MAGNETIC PROPERTIES

The samples for our present spectroscopy study, as well as the crystallographic data used in electronic structure calculations, originate from the the Institute of Organic Chemistry of the University of Erlangen – Nürnberg⁸. The precise chemical formula of the compound in question is $\{M[Fe(L^1)_2]_3\} \cdot 4CHCl_3$, where M is Fe or Cr in the present study. In the following we refer to these systems as FeFe₃ and CrFe₃-stars. The structure of a single molecule derived from crystal structure analysis can be seen in the left panel of Fig. 1, while the spatial packing of the molecules crystallized from chloroform is shown in the right panel. The central iron ion is linked via two μ_2 -alkoxo bridges from each of the three terminal building blocks $[Fe(L^1)_2]^-$. The peripheral iron centers are octahedrally coordinated through two N⁻, μ_1 O⁻, and μ_2 O⁻ donors. All four iron ions are located in a plane, with Fe–Fe–Fe angles of about 120°. As known from the literature, similar types of ferric stars with the FeFe₃– framework can be synthesized using different ligands like dipivaloylmethane (Hdpm) in combination with methanolate or 1,1,1 – tris(hydroxymethyl)ethane (H₃thme), yielding respectively $[Fe_4(OMe)_6(dpm)_6]$ ⁹ or $[Fe_4(thme)_26]$ ¹⁰. The chemistry of $\{M[Fe(L^1)_2]_3\} \cdot 4CHCl_3$ has certain sim-

ilarities with that of “ferric wheels”¹¹, which have the same ligands and a similar (nearly octahedral) coordination of the Fe ions. A relation between the two systems is demonstrated by the fact that adding two equivalents of iron (III) chloride to $[M\{Fe(L^1)_2\}_3]$ produces the known “ferric wheel” with a metallacrown structure as the final product⁸. As in these latter compounds which we have studied earlier^{12,13}, the spins $S=5/2$ of Fe ions tend to couple antiparallel. Contrary to “ferric wheels” with even numbers of Fe atoms, which have zero spin in the ground state, in the “ferric star” the antiparallel coupling of three outer Fe spins to the central one results in a net ground-state spin $S = 3 \times 5/2 - 5/2 = 5$. For the magnetic anisotropy, the effective Hamiltonian of which can be conventionally written in the form $\mathcal{H} = DS_z^2 + E(S_x^2 - S_y^2)$ in terms of the cumulative spin of the molecule, the axial parameter D is -0.20 cm^{-1} (-0.29 K) from the high field electron spin resonance experiments^{9,14}. The absolute value of E (the sign may depend on the definition) was predicted by Kortus to be 0.064 K from a first-principle calculation¹⁵, and later estimated as 0.056 K in experiments by Müller *et al.*¹⁶.

It has been recently demonstrated that Fe in “ferric star” can be substituted by other 3d ions. In the present work we study the spectroscopy of Cr-doped “stars”. The accuracy of the amount and position of the substitution has not yet been unambiguously established. For ab initio calculations we assumed the substitution in the central position, in an otherwise unchanged geometry. A more systematic theoretical analysis of the electronic structure of “ferric wheels” with substitution by different ions in different positions will be reported elsewhere¹⁷.

III. EXPERIMENTAL AND CALCULATION DETAILS

The XPS measurements were performed using a PHI Model 5600ci MultiTechnique system in the Dept. of Physics, University of Osnabrück. The AlK_α radiation was monochromatized by a double focusing monochromator and the pressure during the measurements was typically 10^{-9} mbar. The total energy resolution, as determined at the Fermi level of a gold foil, was 0.3–0.4 eV. The resolution of the electron energy analyzer was 80 meV. The samples were insulating, so charge neutrality on the surface was achieved using a low energy electron flood gun. The recording time of the presented spectra was less than 10 h. The NEXAFS and RIXS measurements were carried out at the BACH beamline of the synchrotron radiation facility in Trieste, using the COMIXS spectrometer^{18,19}.

Normal X-ray emission spectroscopy was performed also at the ROSA beamline at the BESSY II Synchrotron facility in Berlin, using the undulator based beamline ID12-2, and the rotatable spectrometer apparatus (ROSA) at BESSY II, Berlin. The excitation energies were set to 750 eV for the Fe L edge, to 420 eV for the N K edge, and to 600 eV for the O K edge. The overall resolution (beamline plus spectrometer) was set to around 1 eV.

For X-ray photoemission spectroscopy, emitted electron energies were calibrated to the C 1s line from $\text{CH}_2\text{--CH}_2\text{--O}$ ²⁰. For X-ray absorption the resolution was set to 0.3 eV and for emission to 0.7 eV. The emitted photon energies at the iron edge were calibrated to the Fe metal L_α normal emission maximum at 705 eV and at the oxygen K edge to the emission from MgO at 525 eV. The pressure during the measurements was 10^{-9} mbar.

The X-ray photoelectron spectra were recorded of Fe ($3s$, $2p$), C 1s, O 1s, and N 1s core levels. The main peaks of the Fe3s spectra of the “ferric star” were fitted with a Voigt function²¹, by constraining the Gaussian width to a value of 0.6 eV. The background was simulated by a Tougaard function²², and subtracted from the spectra.

The electronic structure of the “ferric stars” was calculated from first principles within the density functional theory, using the calculation method and computer code SIESTA^{23,24,25}. The method uses norm-conserving pseudopotentials in combination with atom-centered strictly confined numerical basis functions^{26,27}. The basis set included double- ζ functions with polarization orbitals added for Fe and O. The treatment of exchange-correlation was done according to the generalized gradient approximation after Perdew–Burke–Ernzerhof²⁸.

The single molecular unit $\{M[\text{Fe}(\text{L}^1)_2]_3\}$ was put into a simulation cell of size $22 \times 22 \times 18$ Å, over which the fast Fourier transform of the charge density has been done with the cutoff 260 Ry. This corresponds to $216 \times 216 \times 180$ divisions along the simulation cell edges, and was tested to be sufficient to obtain converged energy

differences between different magnetic configurations. A discrete energy spectrum was broadened in the following figures with the halfwidth parameter of 0.1 eV in order to get a continuous density of states (DOS). The calculation can be converged to both the ferrimagnetic configuration (the ground state) and the antiferromagnetic configuration (with the spin of one of the outer Fe atoms set parallel to the central one), which is 0.13 eV higher in energy.

IV. ELECTRONIC STRUCTURE AND CHARGE STATE OF Fe

We start with a discussion of electronic structure of the “ferric star” by comparing the spectroscopic data concerning the valence band and first-principles calculations. The XPS spectrum of the valence band is shown in Fig. 2 along with the element-selective X-ray emission spectra of Fe, O, and N. The emission spectra in Fig. 2 correspond to normal non-resonant fluorescence²⁹. Taking into account the binding energies of the corresponding core levels from the XPS (710.76 eV for Fe $2p_{3/2}$, 531.96 eV for O 1s, 400.76 eV for N 1s), the emission spectra were brought to a common energy scale with the valence-band XPS, and they are plotted in Fig. 2. This helps to identify the origin of pronounced features in the valence band. The peak at 6 eV binding energy is mostly due to Fe $3d4s$ states, but the O $2p$ states contribute in about the same region (from ~ 7 eV to higher binding energy). The N $2p$ states are located significantly deeper, forming a broad band centered at about 9 eV binding energy.

These experimental observations are consistent with the results of first-principle calculations, which produce the DOS (summed over both spin directions) as shown in Fig. 3. The top panel depicts the total DOS (summed over both spin directions) in the ground state. Zero energy separates occupied and vacant states. One finds sev-

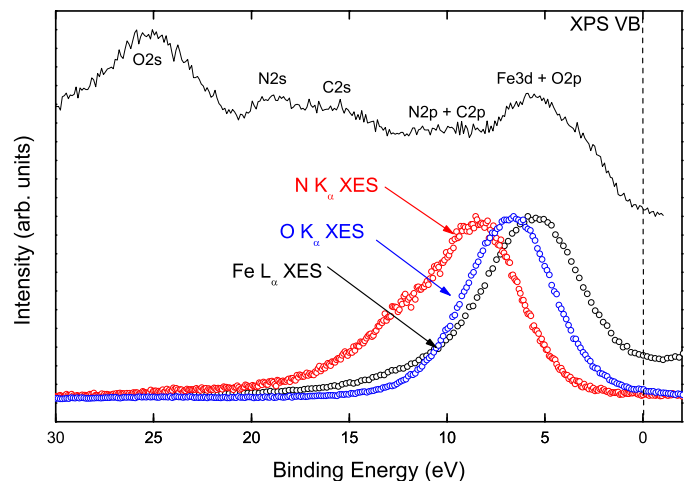


FIG. 2: Valence-band X-ray photoelectron spectrum of the Fe-“ferric star” and X-ray emission spectra of O, N, and Fe.

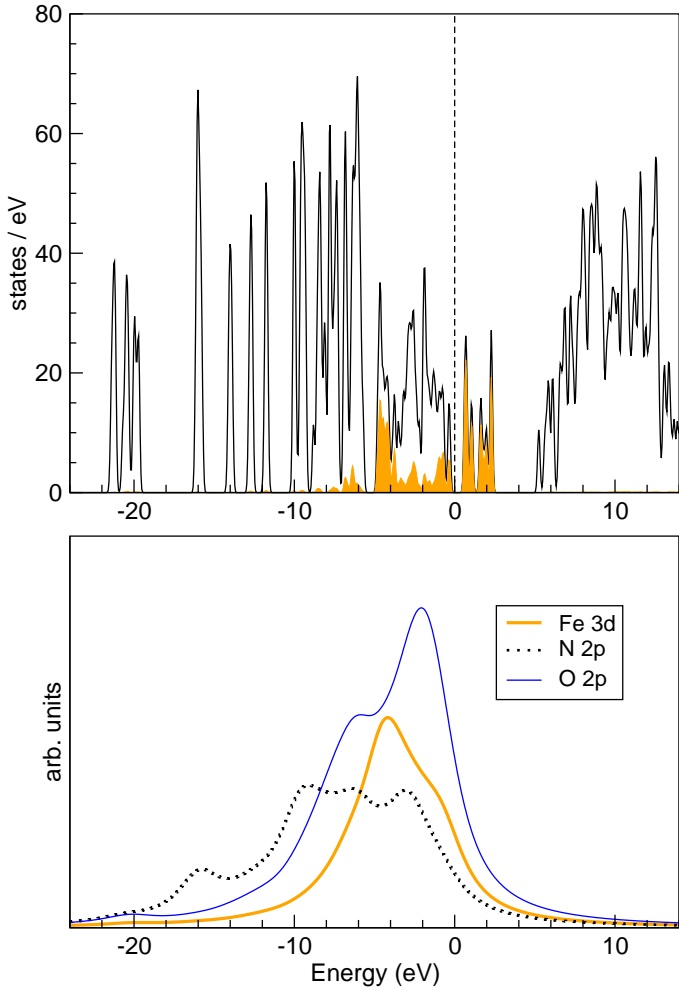


FIG. 3: Top panel: calculated total density of states of the Fe-“ferric star” and local Fe3d density of states (shaded area). Bottom panel: local densities of occupied O2p, Fe3d and N2p states, additionally convoluted with a Lorentzian function of 1.6 eV halfwidth. See text for details.

eral bands, which are derived from the C, N, and O 2s and 2p levels. The lowest compact group of bands around -20 eV is almost exclusively related to O 2s states. The region around the “chemical potential” ($E=0$) hosts Fe 3d states (shown shaded in the figure), which are strongly spin-split (see the discussion below) and strongly hybridize with the O 2p states. There is a “band gap” of ≈ 0.95 eV between the highest occupied and the lowest unoccupied molecular orbitals, both being of mostly Fe 3d–O 2p character in the majority-spin channel (marked spin-down in the following spin-resolved plot). The states with the energies from -16 to -6 eV are all a mixture of different orbitals forming covalent bonds and involving C 2s,2p and N 2s,2p states.

The bottom panel of Fig. 3 shows Fe 3d, N 2p and O 2p contributions, summed up over atoms of the same kind in different positions in the molecule, and over both spin directions; moreover an additional broadening was intro-

duced to yield a more straightforward comparison with the experimental XES of Fig. 2. Indeed these three partial DOS roughly span the states probed by the emission spectra, therefore the comparison is complicated by the lack of structure in the experimental spectra. One notices however a markedly lower energy and much larger width of the N spectrum as compared to other two, in both experiment and theory. The broadness of the N spectrum indicates the participation of N 2p states in a number of molecular orbitals, overlapping with C 2s,2p states throughout the molecule.

Spin-resolved DOS for the atoms in which the spin splitting is pronounced are shown in Fig. 4. A corre-

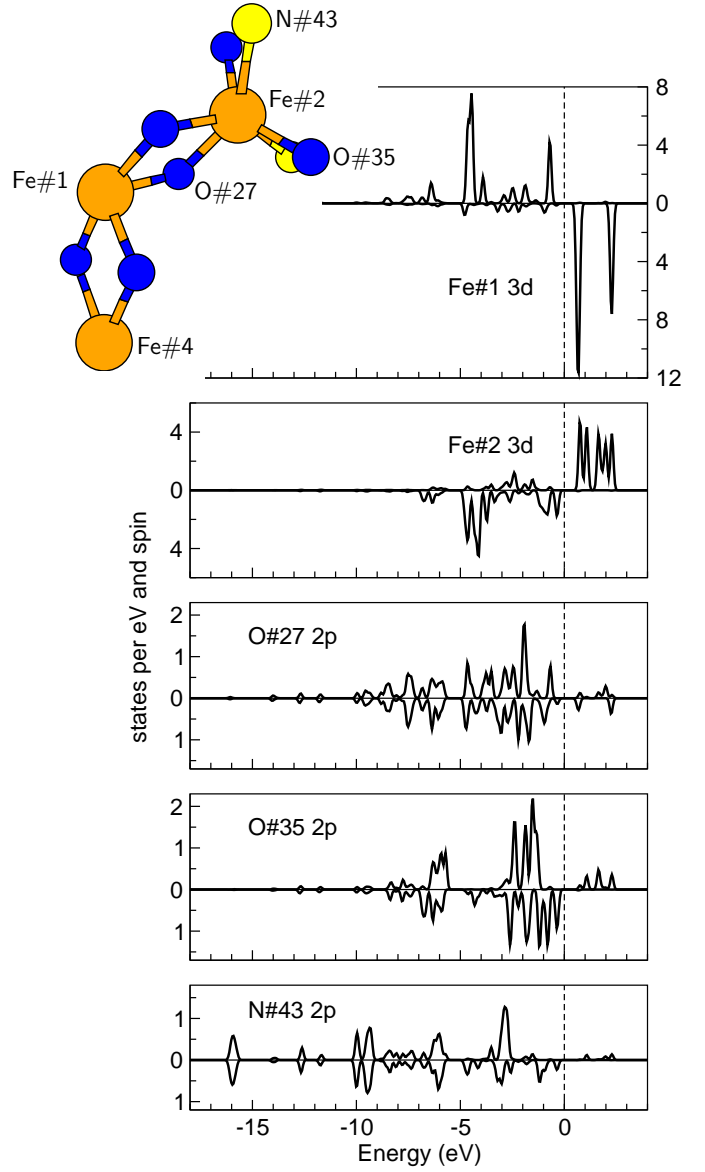


FIG. 4: Spin-resolved local densities of states of two inequivalent Fe sites and some of their nearest neighbors. The numbering of atoms in the relevant fragment of “ferric star” is shown in the inset.

sponding part of the molecule is shown in the inset, with the numbering of atoms. The central atom Fe#1, which has the bridge oxygen atoms (#27) as its only neighbors, carries a magnetic moment of $3.95 \mu_B$. The outer Fe atoms (#2) in the ground state are magnetized oppositely to the central one, with magnetic moments of $-3.93 \mu_B$, and have a different environment, including two N atoms and two O#35. The latter are markedly magnetized, to $-0.26 \mu_B$. The bridge oxygen atoms have a negligible net magnetic moment, but a marked local spin density which changes sign along the path from Fe#1 to O#27 to Fe#2. The induced magnetization at the oxygen atoms adds to the nominal spin moment associated with each Fe atom. The “local” moment of $\sim 4 \mu_B$, which is associated with Fe3d states only, should be increased to $\sim 5 \mu_B$ if one discusses a *distributed* magnetic moment, which in part resides over the ligands, and follows the magnetization flips of its central Fe atom if they occur. Hence, it is a “well-behaved” rigid moment in the sense that the Heisenberg model, or another model dealing with well defined spins, may be applied to it. These observations about the local DOS, induced magnetizations of ligands, and a delocalized but rigid spin moment associated with each Fe site are quite similar to what has been reported earlier for “ferric wheels”, a chemically and structurally related class of molecular magnets^{12,13}.

It is essential to emphasize that bulk techniques (magnetization, magnetic susceptibility) probe the effective spin value, however without addressing its localization. The issue of localization – whether the spin $S=5$ relates strictly to the Fe ion only or extends over ligands – is related to that of nominal valence. Fe³⁺ presumes the maximum-spin $3d^5 d^0$ configuration, whereas Fe²⁺ corresponds to the local magnetic moment of $4 \mu_B$. Core-level spectroscopy, being an element-sensitive method, may permit one to distinguish between these two cases.

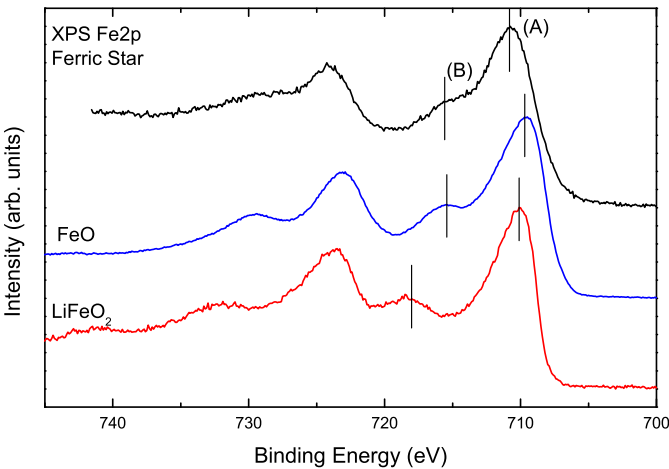


FIG. 5: Fe2p photoelectron spectrum of the Fe-“ferric star” in comparison with those of FeO (definitely Fe²⁺) and LiFeO₂ (definitely Fe³⁺). The features (A) and (B) are discussed in the text.

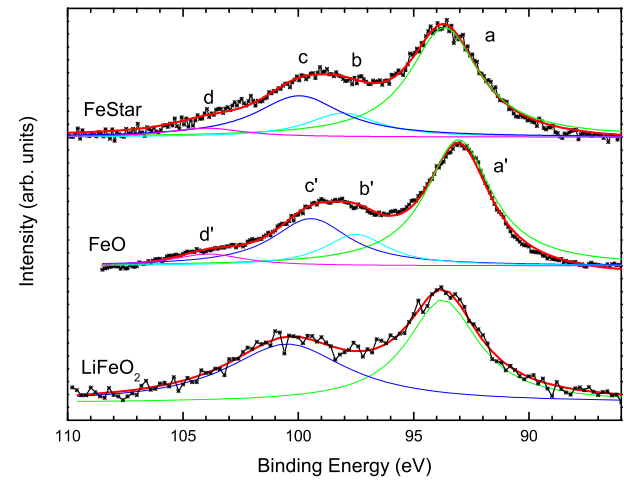


FIG. 6: Fe3s photoelectron spectrum of the Fe-“ferric star” in comparison with those of FeO (definitely Fe²⁺) and LiFeO₂ (definitely Fe³⁺). The features (a), (b), (c) and (d) are discussed in the text.

Fig. 5 depicts the $2p_{3/2}$ and $2p_{1/2}$ photoelectron spectra of the “ferric star” along with those of two benchmark compounds, of well-known Fe²⁺ and Fe³⁺ valence: FeO, similar to what was earlier discussed in ref.³⁰ and LiFeO₂³¹, respectively. Characteristic ligand-to-metal charge-transfer effects are present in the Fe 2p spectra of the Fe “ferric star”, as well as in the spectra of FeO and LiFeO₂, yet there are some dissimilarities between these two reference systems. The relative positions and widths of the peaks due to the final state with charge transfer $2p^5 3d^{n+1} \underline{L}$ (A) and that without charge transfer $2p^5 3d^n L$ (B) in the spectrum of “ferric star” is similar to that of the FeO which indicates the Fe²⁺ valence state.

The 3s core-level photoelectron spectra of the “ferric star”, again in comparison with those of FeO and LiFeO₂, are shown in Fig. 6. The spectrum of the “ferric star” consists of two well separated peaks (a) and (c), according to whether the spin of the emitted 3s core electron is parallel or antiparallel to that of the 3d shell. Each of these peaks has a satellite denoted with (b) and (d), satellites which were assigned by Sangalli and Pamigiani³² in the case of FeO to charge transfer excitations, with corresponding peaks labelled a', b', c' and d'.

In LiFeO₂ the charge transfer is not prominent, therefore the fitting was done using two peaks only. The splitting is proportional to the number of unpaired d electrons and hence to total spin S ; the predicted relative intensities are given by the relation $S/(S+1)$ ³³. The value of the Fe 3s splitting in the case of the “ferric star” is about 5.10 eV, to be compared to 5.5 eV in FeO and 6.5 eV in LiFeO₂. We conclude that a nominal valence Fe²⁺ is more plausible in the “ferric star”.

V. RESONANT X-RAY EMISSION IN PURE AND Cr-DOPED FERRIC STARS

We turn now to the comparative analysis of pure and Cr-doped systems. The Cr substitution site is not unambiguously determined by experiment, whereas recent first-principle calculations presume that it must be the central one³⁴. The valence-band XPS and Fe L -emission spectra are very similar in both systems, and Cr-related features cannot be resolved. However, certain differences were found when analyzing resonant X-ray emission, see Figs. 7 and 8. Panel (a) of Fig. 7 depicts the NEXAFS spectrum of the “ferric star” with $M=\text{Fe}$, covering the Fe $L_{2,3}$ edges. The peak at about 709 eV corresponds to the (L_3) excitations from the Fe $2p_{3/2}$ core state into the unoccupied $3d$ band, and the second one at about 721 eV corresponds to those (L_2) from the Fe $2p_{1/2}$ state. The asymmetry seen in the first structure is very similar to that observed for FeO, which has been explained in terms of many overlapping multiplets³⁵. When comparing this two-peaked structure with the XPS, we note that here the L_2-L_3 splitting is 12.73 eV, i.e. less than the spin-orbit splitting of the Fe $2p$ states determined by XPS (14 eV). The reason for the discrepancy is that the both the XPS and absorption spectra consist of many

multiplets, but these multiplets are different for the ionic (XPS) and neutral (absorption) final states, and therefore have different splittings. Panel (b) of Fig. 7 shows the X-ray emission spectra at the L_3 edge, obtained for four different incident photon energies: 719.02, 719.25, 720, and 720.9 eV. Their positions at the threshold and on the top of the L_2 edge are indicated in the panel with the absorption spectrum.

In RIXS, a $2p \rightarrow \text{CB}$ (CB: conduction band) excitation is followed by a $\text{VB} \rightarrow 2p$ (VB: valence band) X-ray emission; both events are normally treated as a single joint process. As the excitation energy is gradually increased, on reaching the L_3 absorption threshold the L_α emission ($3d \rightarrow 2p_{3/2}$) becomes possible. As the incident photon energy approaches the L_2 threshold, the L_β emission ($3d \rightarrow 2p_{1/2}$) appears as well. The L_α emission persists, as an off-resonance scattering process (creation and annihilation of a $2p_{3/2}$ hole), but also possible by a Coster–Kronig process. In the latter, an initial $2p_{1/2}$ hole is filled due to a radiationless $2p_{3/2} \rightarrow 2p_{1/2}$ transition, and the resulting $2p_{3/2}$ hole is filled by L_α emission. These different mechanisms affect the L_α/L_β intensity ratio as a function of the excitation energy. We note that the FeFe_3 and CrFe_3 stars, in spite of many similarities in their $\text{Fe}L$ spectra, behave markedly differently in what regards the

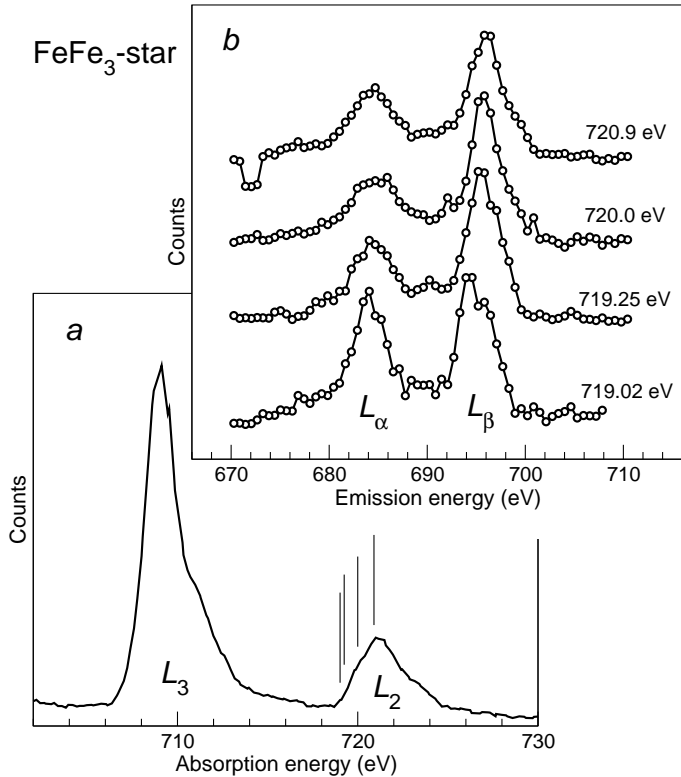


FIG. 7: Near-edge X-ray absorption Fe $L_{2,3}$ spectrum (a) and resonant inelastic X-ray Fe L_3 emission spectra (b) of the Fe-“ferric star” for four selected excitation energies, which are also shown in the bottom panel as vertical bars. See text for details.

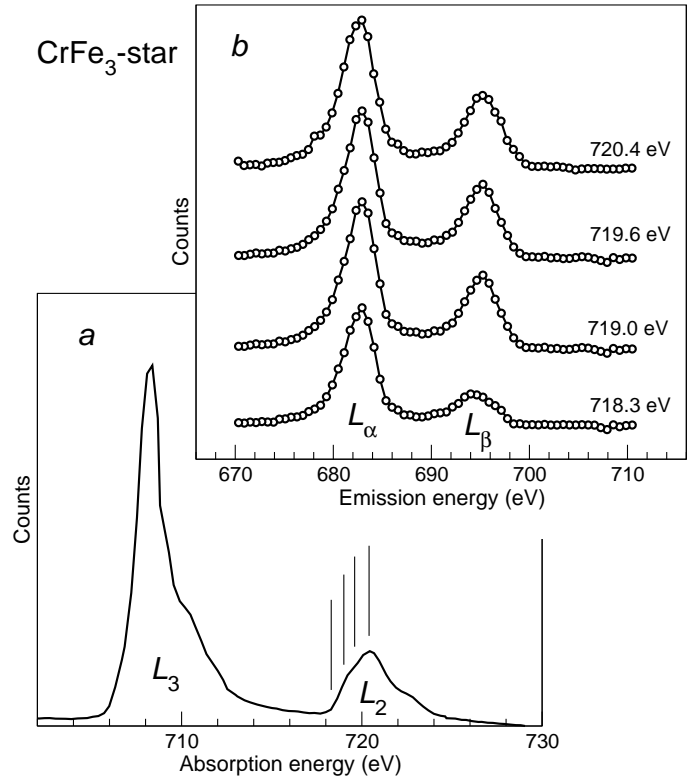


FIG. 8: Near-edge X-ray absorption Fe $L_{2,3}$ spectrum (a) and resonant inelastic X-ray Fe L_3 emission spectra (b) of the Cr-“ferric star” for four selected excitation energies, which are also shown in the bottom panel as vertical bars. See text for details.

L_α/L_β intensity ratio on passing through the L_2 resonance excitation. In Fig. 7(b) we observe that at the maximum of the absorption resonance, the L_β intensity is higher than that of L_α . We will see that this behavior is different from the L_α/L_β intensity ratio which occurs in the case of Cr substitution in the "ferric star".

Fig. 8(a) depicts the NEXAFS at the Fe $L_{2,3}$ edge for the Cr-doped sample, and Fig. 8(b) – the X-ray emission spectra, taken at the resonance energies 718.3, 719, 719.6 and 720.4 eV, from the onset to the maximum of the L_2 absorption. The intensity of the L_β emission first grows and then remains constant, relative to that of L_α . The same behavior has been observed and discussed for the case of FeO, in contrast to (non-magnetic) FeS₂, by Prince *et al.*³³. Another example of such behavior was reported for Mn L RIXS spectra in Heusler alloys³⁶. The interpretation of results in these papers related the L_α/L_β intensity to the high-spin state of Fe or Mn. More specifically, the importance of having an electronic structure with the majority-spin band occupied and the minority-spin band empty was emphasized. In this case a sequence of two processes, which may involve a Coster-Kronig transition as an intermediate step – an electron excitation into the CB and filling of the core hole by an electron from the VB – cannot occur except with the inversion of spin, which is a low-probability event. On the contrary, the electron excitation into the CB and an immediate fluorescence transition, which is a resonance process, remains allowed and explains the dominance of the L_β emission on L_2 excitation.

It is known that Coster-Kronig transition rates are also affected by chemical environment. For example in the case of Te³⁷, changing the chemical environment drastically from metallic to oxides to organometallic compounds produced a variation of 23 % in the ratio of the widths of the $3p_{3/2}$ to $3p_{1/2}$ peaks. In the present case, the chemical environment is very similar so we expect small chemical effects. However the L_α/L_β branching ratio changes by 2, which is a large effect similar to that in³³ where the changes was nearly a factor of 3. We therefore correlated the large change observed to changes in magnetic properties.

Fig. 4 makes clear that the local Fe DOS in the "ferric star" looks like that in a strong magnet, with the majority-spin band fully occupied, and only a small contribution (due to hybridization with O 2p states) present in the occupied part of the minority-spin channel. Therefore the RIXS spectra in the FeFe₃-star can be explained consistently with that in FeO or in Heusler alloys. The situation with the CrFe₃-star, as is seen from the calculated local DOS shown in Fig. 9, is different: whereas the Fe local DOS (of the peripheral atoms, compare to Fig. 4) is identical to that in the FeFe₃-star, the majority-spin states centered at the Cr site are not fully occupied. Moreover the lowest unoccupied states appear in the majority-spin channel. Therefore the absorption-emission processes involving the Cr 3d states may happen without the inversion of spin³⁸. However, we admit that

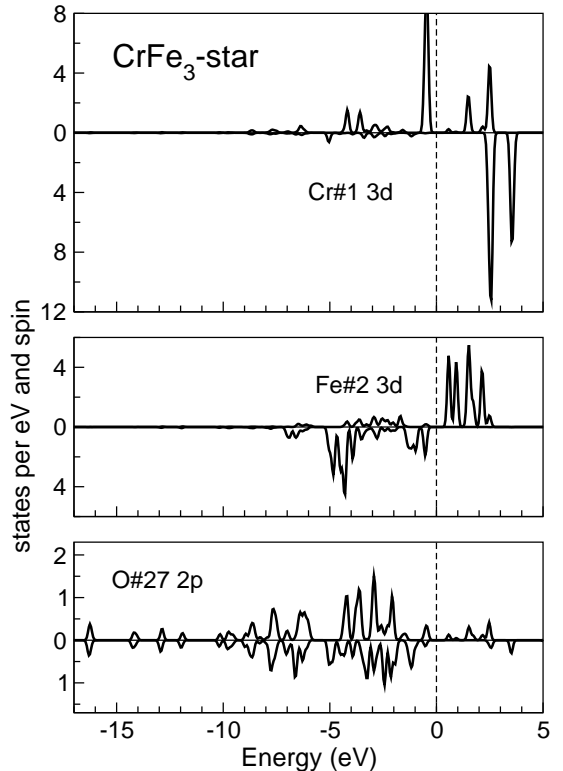


FIG. 9: Spin-resolved local densities of states of Cr, Fe and the bridging oxygen in the CrFe₃-star, to be compared to Fig. 4.

it is difficult to understand how this fact helps to reduce an apparent blocking of the Coster-Kronig transitions *at the Fe site*. Some clue may be provided by considering the bridging oxygen atoms (#27 of Fig. 4): whereas in the FeFe₃-star the magnetization density changes its sign exactly at the bridging O, in the CrFe₃-star this oxygen atom is fully magnetized along with its Fe neighbor, and oppositely to Cr. One can speculate that the matrix elements of the core-valence transitions, which include differently composed molecular orbitals in the valence band of FeFe₃- and CrFe₃-stars, may affect relative weights of L_α and L_β emission. This is however difficult to estimate without an explicit calculation of the RIXS process.

We can, with relative certainty, eliminate the following other hypothetical explanations of a different behavior in the L_α/L_β intensity ratio of the CrFe₃-star. A possibility of a low-spin state is ruled out by the calculation result that in all trial spin-polarized calculations, the local magnetic moments remained essentially fixed to $\approx 3 \mu_B$ at the Cr site and $\approx 4 \mu_B$ at Fe sites. There is no way to "prepare" the system with a low-spin state of either Cr, or Fe¹⁷. All inversions of individual local moments from the ground state, including the situation with the lowest total magnetic moment of 2 μ_B in the Cr_↑Fe_↓Fe_↓Fe_↑ star, preserve the "strong magnetism" at the Fe site and the partial emptiness of the majority-spin states at the Cr site, with strong similarities of their corresponding DOS

to those shown in Figs. 4 and 9. Also the assumed Cr substitution in the peripheral position (highly energetically unfavorable, as was mentioned above) affected the magnetic moments and local DOS only slightly. An additional inclusion of on-site intraatomic Coulomb correlation beyond the conventional DFT treatment may affect the energy placements of $3d$ levels in the Cr and Fe DOS, but it can only enhance the “strong magnetism” at the Fe site rather than ease it, in the presence of Cr dopant.

Therefore the understanding of L_α/L_β behavior in the CrFe₃-star is incomplete on the basis of DFT calculations, whereas an explanation of the behavior in FeFe₃-star seems rather obvious, and consistent with the observed trend³³ for FeO, as compared to FeS₂. We can only emphasize the observed difference in RIXS spectra of FeFe₃- and CrFe₃-stars as an experimental finding, which might stimulate additional research on these systems.

VI. CONCLUSIONS

We have reported photoemission and photoabsorption spectra of $\{M[Fe(L^1)2]3\} \cdot 4CHCl_3$ ($M = Fe, Cr$) in comparison with first-principles electronic structure calculations. First we determined the charge state of Fe in these “ferric stars”, in view of an existing controversy between the expected nominal chemical valence (Fe III), from one side, and the calculated value of the Fe local magnetic moment ($4 \mu_B$), that would imply a bivalent iron, from the other side. On the basis of a comparison of the Fe $2p$ and $3s$ photoelectron spectra with those of reference compounds, the charge state of Fe in the FeFe₃-star was argued to be 2^+ . The valence-band X-ray photoelectron

spectrum and the X-ray Fe L , O and NK emission spectra show little structure but are otherwise in agreement with DFT calculations. In the FeFe₃- and CrFe₃-stars, the L_α/L_β intensity ratio in resonant X-ray emission, varies according to the excitation energy on going through the Fe L_2 threshold. The trend observed in the FeFe₃-star is similar to that earlier reported by Yablonskikh *et al.* and Prince *et al.*, and believed to be a signature of “high-spin” structures, or more precisely of strong magnetic systems, like e.g. FeO or Heusler alloys. The explanation of this behavior is consistent with the assumption that the Coster–Kronig process probability is suppressed in strong magnets. The DFT calculation does indeed support an assumption of such strong magnetic behavior in the FeFe₃-star. However, the CrFe₃-star does not show such a trend in the L_α/L_β intensity, even though the local electronic structure at the Fe site remains largely the same as in the FeFe₃-star, and the loss of strong magnetic character appears confined to the Cr center.

Acknowledgments

AVP, AS, and SS gratefully acknowledge the financial support by the Deutsche Forschungsgemeinschaft (SPP 1137 ‘Molecular Magnets’), AT and KK acknowledge financial support of the PhD program of Lower Saxony (Germany). Many enlightening discussions with P. Müller, R. Fink and S. Blügel are appreciated. We thank J. Kortus for making available for comparison the unpublished results of his *ab initio* calculations on the ferric stars, which have been done prior to those of the present work. We thank the beamline scientists from the BACH beamline (ELETTRA) for the overall excellent support which they provided.

* Electronic address: altakacs@uni-osnabrueck.de

† Electronic address: apostnik@uos.de

¹ M. Verdaguer, A. Bleuzen, C. Train, R. Garde, F. Fabrizi de Biani, and C. Desplanches, *Phil. Trans. R. Soc. Lond. A* **357**, 2959 (1999).

² M. N. Leuenberger and D. Loss, *Nature* **410**, 789 (2001).

³ S.-i. Ohkoshi and K. Hashimoto, *The Electrochemical Society Interface* **11**, 34 (2002).

⁴ O. Kahn, *Molecular Magnetism* (John Wiley & Sons, Singapore, 1993), ISBN 0-471-18838-7.

⁵ W. Linert and M. Verdaguer, eds., *Molecular Magnets* (Springer-Verlag, Wien, 2003), ISBN ISBN: 3-211-83891-0, special Edition of Monatshefte für Chemie/Chemical Monthly, Vol. 134, No. 2.

⁶ J. S. Miller and A. J. Epstein, *MRS Bulletin* **25**, 21 (2000).

⁷ S. J. Blundell and F. L. Pratt, *J. Phys.: Condens. Matter* **16**, R771 (2004).

⁸ R. W. Saalfrank, I. Bernt, M. M. Chowdhry, F. Hampel, and G. B. M. Vaughan, *Chem. Eur. J.* **7**, 2765 (2001).

⁹ A. L. Barra, A. Caneschi, A. Cornia, F. Fabrizi de Biani, D. Gatteschi, C. Sangregorio, R. Sessoli, and L. Sorace, *J. Am. Chem. Soc.* **121**, 5302 (1999).

¹⁰ A. Cornia, A. C. Fabretti, P. Garrisi, C. Mortalo, D. Bonacchi, D. Gatteschi, R. Sessoli, L. Sorace, W. Wernsdorfer, and A. L. Barra, *Angewandte Chemie – International Edition* **43**, 1136 (2004).

¹¹ R. W. Saalfrank, I. Bernt, E. Uller, and F. Hampel, *Angewandte Chemie – International Edition* **36**, 2482 (1997).

¹² A. V. Postnikov, S. G. Chiuzbăian, M. Neumann, and S. Blügel, *J. Phys. Chem. Solids* **65**, 813 (2004).

¹³ A. V. Postnikov, J. Kortus, and S. Blügel, *Molecular Physics Reports* **38**, 56 (2003).

¹⁴ D. Gatteschi, R. Sessoli, and A. Cornia, *Chem. Commun.* p. 725 (2000).

¹⁵ J. Kortus (unpublished).

¹⁶ R. Koch, S. Schromm, H. Rupp, and P. Müller, private communication.

¹⁷ A. V. Postnikov and S. Blügel, to be published.

¹⁸ M. Zangrandi, M. Finazzi, G. Polucci, G. Comelli, B. Di-ciacco, R. P. Walker, D. Cocco, and F. Parmigiani, *Rev. Sci. Instrum.* **72**, 1313 (2001).

¹⁹ D. Cocco, M. Matteucci, K. Prince, and M. Zangrandi, *Proceedings SPIE* **4506** (2001).

²⁰ G. Beamson and D. Briggs, eds., *High Resolution XPS of*

Organic Polymers: The Scienta ESCA300 Database (John Wiley & Sons, Chichester, 1992).

²¹ S. Doniach and M. Šunjić, *Journal of Physics C* **3**, 285 (1970).

²² S. Tougaard, *Surface and Interface Analysis* **11**, 453 (1988).

²³ P. Ordejón, E. Artacho, and J. M. Soler, *Phys. Rev. B* **53**, R10441 (1996).

²⁴ J. M. Soler, E. Artacho, J. D. Gale, A. García, J. Junquera, P. Ordejón, and D. Sánchez-Portal, *J. Phys.: Condens. Matter* **14**, 2745 (2002).

²⁵ URL <http://www.uam.es/siesta>.

²⁶ D. Sánchez-Portal, E. Artacho, and J. M. Soler, *J. Phys.: Condens. Matter* **8**, 3859 (1996).

²⁷ J. Junquera, Ó. Paz, D. Sánchez-Portal, and E. Artacho, *Phys. Rev. B* **64**, 235111 (2001).

²⁸ J. P. Perdew, K. Burke, and M. Ernzerhof, *Phys. Rev. Lett.* **77**, 3865 (1996).

²⁹ R. Szargan, K.-H. Hallmeier, R. Hesse, A. Kopczynski, S. A. Krasnikov, L. Zhang, T. Chassé, O. Fuchs, C. Heske, and E. Umbach, *X-ray fluorescence spectroscopy at U41-PGM by means of ROSA—present status and results*, BESSY Annual Report 2001.

³⁰ B. Mayer, S. Uhlenbrock, and M. Neumann, *J. Electron. Spectrosc. Relat. Phenom.* **81**, 63 (1996).

³¹ V. R. Galakhov, A. I. Poteryaev, E. Z. Kurmaev, V. I. Anisimov, S. Bartkowski, M. Neumann, Z. W. Lu, B. M. Klein, and T.-R. Zhao, *Phys. Rev. B* **56**, 4584 (1997).

³² F. Parmigiani and L. Sangaletti, *J. Electron Spectrosc. Relat. Phenom.* **98–99**, 287 (1999).

³³ K. C. Prince, M. Matteucci, K. Kuepper, S. G. Chiuzbâian, S. Bartkowski, and M. Neumann, *Phys. Rev. B* **71**, 085102 (2005).

³⁴ According to our recent calculations, the central position of substitutional Cr is by 1 eV/molecule more favorable than the peripheral one.

³⁵ J. P. Crocombette, M. Pollak, F. Jollet, N. Thromat, and M. Gautier-Soyer, *Phys. Rev. B* **52**, 3143 (1995).

³⁶ M. V. Yablonskikh, Y. M. Yarmoshenko, V. I. Grebenikov, E. Z. Kurmaev, S. M. Butorin, L.-C. Duda, J. Nordgren, S. Plogmann, and M. Neumann, *Phys. Rev. B* **63**, 235117 (2001).

³⁷ M. K. Bahl, R. L. Watson, and K. J. Irgolic, *J. Phys. Chem.* **66**, 5526 (1977).

³⁸ We emphasize that the occupation of Fe or Cr states in the FeCr₃ star remains qualitatively the same also for other possible configurations: when the Cr atom substitutes a peripheral site, or with different setting of magnetization directions over Fe, Cr atoms.